2018 IEEE International Conference on Robotics and Automation (ICRA)
May 21-25, 2018, Brisbane, Australia

Fore-Aft Leg Specialization Controller for a Dynamic Quadruped

Jason M. Brown[13], Charlie P. Carbiener[13], John Nicholson[1],
Nicholas Hemenway[1], Jason L. Pusey[2], Jonathan E. Clark[1]

***Abstract*— Many running animals, unlike their robotic counterparts, have distinct morphologies and functional roles for their front and rear legs. In this paper we present a new control approach for a $5kg$ autonomous dynamic quadruped that explicitly encodes separate roles for each contralateral pair of legs. This controller utilizes a functional dynamic decomposition similar to Raibert's three part control law, but focuses on fore-aft leg specialization to regulate the robot's performance. The velocity of this controller, which exceeds 5 body lengths per sec, is compared with an improved trajectory-based controller and shown to be significantly more robust to changes in environment.**

I. Introduction

With the ability to quickly and effectively navigate across varying terrain, animals still currently demonstrate the state of the art in legged locomotion. Roboticists have worked to emulate this performance by capturing the underlying dynamics [1], [2] demonstrated by animals and then embed these in the physical structure and control of robotic platforms.

The fundamental dynamics of many large biological runners is captured by a single spring loaded inverted pendulum (SLIP) model [3], [4]. Because this model is instantiated by hopping monopedal robots, numerous controllers have been developed which handle the control of a single leg [2], [5], [6]. With the development of multi-legged robotics with multi degree of freedom (DOF) legs, such as MIT's Cheetahs [7], Boston Dynamics' BigDog [8], ANYmal [9], and Minitaur [10] (shown in Fig. 1a), controllers have been expanded to handle regulating the additional body DOFs.

While other researchers have explored implementing unique leg coordination controllers [11], [12], the individual leg controllers for these multi-legged platforms can be grouped into a few distinct classes. The first of these prescribes the Center of Mass (COM) trajectory, solves the inverse dynamics problem, and maps the analytically determined body forces to the leg outputs. This approach, demonstrated on the MIT Cheetah [13] and ANYmal [14], is computationally expensive and has stringent sensing requirements, but enables explicit control of body trajectory.

A second class allows the COM motion to emerge from the leg actuation scheme coupled with the passive dynamics. Within this second class are two distinct approaches, limb prescribed feed-forward foot trajectories which the passive dynamics mitigate to create stable COM motions (implementations include Rhex [15], Minitaur [16]) and a functional dynamic decomposition which maps the aspects of the passive dynamics to parts of the control policy (the approach used by Raibert to the achieve first running quadrupedal gaits [17]). Both of these approaches are computationally very efficient and do not run the risk of fighting against the systems' natural dynamics, but only the functional dynamic decomposition inherently enables the controller to automatically adjust to varied environmental conditions.

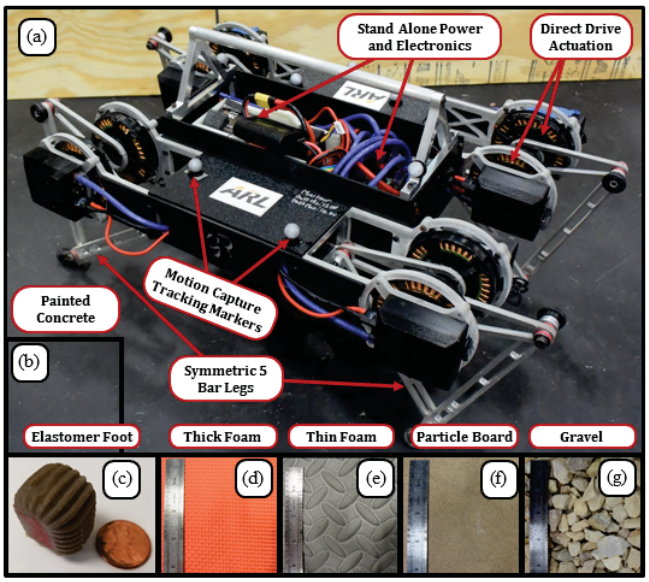

Fig. 1: a) Minitaur Robot, which uses symmetric 5 bar legs via direct drive actuation. Additionally, Minitaur has onboard power and electronics that allow it to run completely untethered. b) Painted concrete surface with Minitaur included for scale. c) Improved cast elastomer feet with ribbed groves for improved traction. d-g). Additional surfaces (Thick Foam, Thin Foam, Smooth Particle Board and Compacted Gravel respectively) tested with a 4 inch ruler shown for scale.

The functional dynamic decomposition used by Raibert mapped the dynamics of the quadruped to a single virtual leg, which the physical legs were then slaved to.

For quadrupeds and hexapods, another type of functional decomposition (fore-aft leg specialization) is possible, and is inspired by biological runners. Cockroaches, for example, have been shown to use their front and rear legs differently, with the front legs providing a braking and lifting force while the rear legs provide primarily a thrusting force [18],

[1] Department of Mechanical Engineering, Florida State University, Tallahassee, FL, 32310 USA e-mail: jmb10t@my.fsu.edu.
[2] U.S. Army Research Laboratory - Vehicle Technology Directorate - Autonomous Systems Division e-mail: jason.l.pusey.civ@mail.mil
[3] These Authors Contributed Equally to this work

[19]. For the cockroach, this is partially accomplished with a fore-aft sprawled kinematic posture, where the front legs are upright and the rear legs are placed behind the body.

Previously, this leg role specialization has been implemented kinematically on the Sprawl family of robots [20], [21], which at the time achieved the fastest running velocity of over 15 BL/s [22]. The Sprawl robots used prismatic actuation, fixed, but distinct, leg angles for the front and rear legs, and finely tuned torsional springs to achieve this rapid locomotion.

The limitation of the sprawl robots morphology with only a single active degree of freedom required the design to compromise between speed and stability. Minitaur, shown in Fig. 1a, on the other hand, despite limited computation and sensing capabilities, has 2 degree of freedom (DOF) legs and is capable of individually altering the front and rear leg control while dynamically running [10]. Minitaur uses a unique five-bar leg design enabling the legs to be directly driven by the motors (motors without gearboxes). Because of this design, the motor inertia is not amplified by a gearbox and this motor transparency enables the motors to behave as tunable torsional springs. These springs can then be mapped to a virtual torsional and prismatic spring via the manipulator Jacobian [14]. These design features enable the implementation of intra-stride stiffness variation.

In this paper, we examine two emergent dynamics controllers for Minitaur, an improved feed-forward trajectory controller and a new functional leg specialization controller. The concept of functional leg specialization is utilized to define a distinct dynamic decomposition, and a unique implementation of this control approach is presented in section II. In section III, this controller design is analyzed via reduced order simulation, and then in section IV the performance and robustness of the new controller is tested experimentally against the improved trajectory controller over various terrain surfaces. Sections V and VI describe and discuss the results of these experiments and some concluding results and future directions are given in section VII.

II. Controller Design

A. Trajectory Controller

To evaluate the performance improvement of the new controller, a baseline controller was required. The previously implemented trajectory based controller, shown as the blue quadrangle on Fig. 2, was selected as it has been shown to achieve the fastest gaits on Minitaur [16]. The trajectory controller operates by prescribing a feed forward foot trajectory that each foot follows at a fixed timing offset from a reference leg.

Previously implemented trajectories used a minimal set of points (3 and 4) to define the shape of the trajectory, with linear segments between each leg. The touchdown approach angle β and the stroke length L_{stroke} were found to be key parameters in optimizing the speed [16], [23]. While these controllers achieved speeds up to 1.9 m/s, here we improve the gait by applying similar techniques as used by Hyun et. al [13] to smooth the trajectory. In this paper, we use

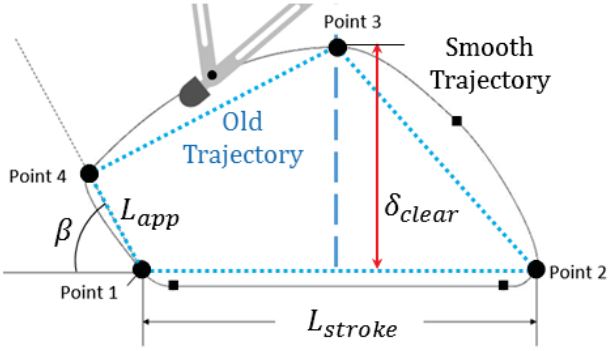

Fig. 2: Overlay of the previous control design (linear segments shown in blue) and the improved trajectory control which smooths the previous trajectory using polynomial splines (gray lines the foot tracks).

a polynomial spline which enabled the control points to be directly included in the trajectory, shown as the gray lines of Fig. 2. This allows us to prescribe the smooth trajectory with just 4 parameters (L_{stroke}, β,δ_{clear}, and L_{app}).

B. New Dynamic Controller Design Concept

In this section we describe the new fore-aft leg specialization controller. Rather than focusing on prescribing a trajectory for the feet, this controller decomposes portions of the control task to the front and rear legs respectively. This functional decomposition using leg specialization creates a unique mapping between leg behavior and body dynamics. Much like the three-part control law developed by Raibert, which correlates touchdown (TD) angle to body velocity, thrust magnitude to hop height, and hip torque to pitch control [2], with our new controller, the front legs are responsible for braking and pertubation recovery and the rear legs are responsible for generating forward thrust. Leg actuation amplitude is also used to regulate body pitch. Each of these three concepts are described below. The integration of these results in the new controller called the Leg Specialization Controller, or LSC.

C. Rear Leg Control Design

Within the LSC, the primary role of the rear legs is to generate forward thrust by prismatically extending the legs. The horizontal thrust generated by the rear legs is modulated by changing the rear TD angle as illustrated by Fig 3a. and is defined by Eq. 1, which modifies the next touchdown angle TD_{n+1_r} from the current TD angle TD_{n_r} by a fixed amount δ on a step to step basis, based on the force torque ratio flag τ_{ratio}. This force torque ratio was implemented in lieu of a slip measurement as slip measurement required additional sensing not currently available on Minitaur.

$$TD_{n+1_r} = TD_{n_r} + \tau_{ratio} * \delta \tag{1}$$

The force torque ratio, given in Eq. 2, is set to -1 (which will decrease the next desired TD angle) if the amount of torque from the virtual torsional spring at the hip τ_{hip} divided

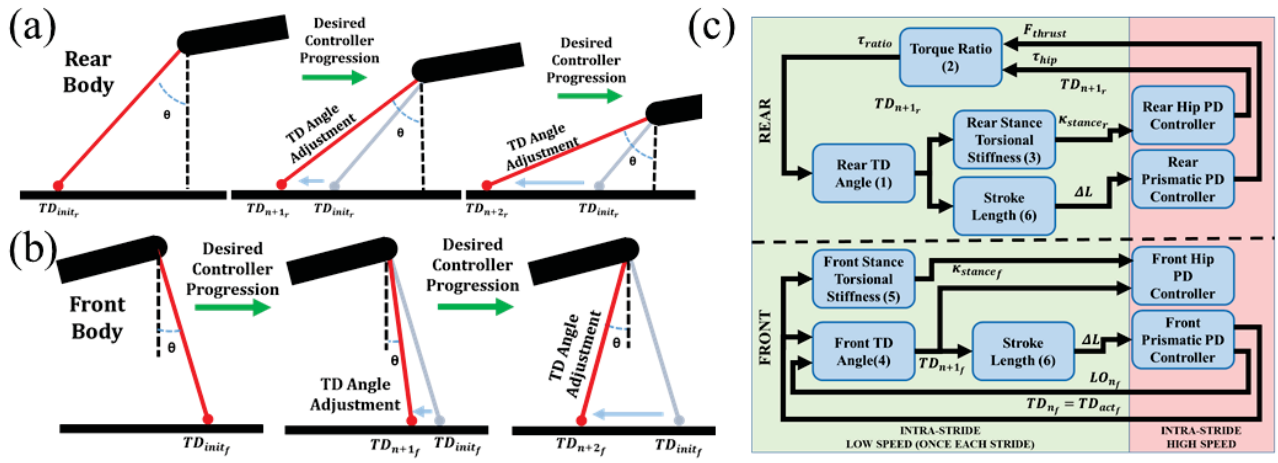

Fig. 3: Illustration of the conceptual goals of each component of new controller. a). The goal of the rear leg controller is to maximize horizontal thrust by modulating the touchdown angle. b). The goal of the front controller is to provide the minimum amount of braking force (needed for stability) by regulating the touchdown angle. c). Flow chart outlining the actual controller implementation. The controller parts are decoupled but use the same stroke length equation to regulate body pitch.

by the amount of thrusting force F_{thrust} produced exceeds some threshold at any time during the previous step. While the torsional spring provides lift for the rear legs, it also produces an undesirable braking force. Thus, to maximize the overall thrust generated by the rear legs, this ratio should be small.

$$\tau_{ratio} = \begin{cases} -1, & \text{if } \frac{\tau_{hip}}{F_{thrust}} > threshold \\ 1, & otherwise \end{cases} \quad (2)$$

As the leg is set further behind the body, the amount of vertical thrust provided by the extension of the legs and the rear hip height decreases. To compensate for this, the torsional spring stiffness in the rear is increased based on Eq. 3, which increases the torsional stiffnesses, κ_{stance_r}, linearly from an initial stiffness, κ_{init_r}, at a rate defined by the controller gain c_3 as the TD angle is set further back from the initial TD angle, TD_{init_r}.

$$\kappa_{stance_r} = \kappa_{init_r}(c_3(TD_{n+1_r} - TD_{init_r}) + TD_{init_r}) \quad (3)$$

D. Front Leg Control Design

The primary role of the front legs is to provide a lifting force which keeps the body from falling forward and a braking force to provide stability. The braking force generated by the front legs is regulated by changing the front TD angle, as illustrated in Fig. 3b and defined by:

$$TD_{n+1_f} = TD_{init_f} - c_1(TD_{n_f} - LO_{n_f}) \quad (4)$$

Eq. 4 reduces the next touchdown angle, TD_{n+1_f}, based on the amount of sweep experienced in the last step (the last TD angle TD_{n_f} minus the last liftoff angle LO_{n_f}) scaled by a tuned controller gain c_1. However, since the initial TD angle, TD_{init_f}, is a constant rather than TD_n, this is not a standard feedback control, which would result in a purely positive feedback loop.

While Eq. 4 does not result in a traditional positive feedback loop, there is no mechanism to determine if sufficient braking is added for stability purposes, or more importantly a recovery mechanism if the system trips where touchdown then occurs prior to having sufficient time to recirculate the leg. Thus, Eq. 5 adds a safety and stability mechanism in the form of a torsional spring if the leg touches down prior to fully recirculating, with the spring stiffness, κ_{stance_f}, equal to the difference in desired front TD angle TD_{des_f} and the actual front TD angle TD_{act_f} scaled by a controller gain c_2.

$$\kappa_{stance_f} = \begin{cases} c_2(TD_{des_f} - TD_{act_f}) & \text{if } (TD_{des_f} - TD_{act_f}) \geq 0 \\ 0 & \text{otherwise} \end{cases} \quad (5)$$

Adding a torsional spring at the hip significantly increases the braking force and adds a lifting force, which prevents the robot from falling forward. This safety mechanism is possible because Minitaur uses virtual springs produced via low level controller gains.

E. Whole Body Pitch Regulation

To provide pitching regulation, the actuation amplitude of the sinusoidal leg thrusting for the front and rear legs, ΔL , is defined to kinematically travel the same distance in the vertical direction, ΔL_{vert} :

$$\Delta L = \frac{\Delta L_{vert}}{\cos(TD_{n+1})} \quad (6)$$

This results in larger actuation amplitudes for the rear leg as the TD angle is set further back as shown in Fig. 4a.

F. Overall Implementation

The overall implementation of this controller is summarized in Fig. 3c. TD and LO events are determined by approximating the force in the leg with low level controller errors, where TD occurs when this error exceeds some threshold and LO occurs ending the stance phase when the error drops below the same threshold. Once in flight, the prismatic actuation follows a prescribed trajectory while the angular actuation behaves as a torsional spring with the nominal point instantaneously placed at the next TD angle at the moment of liftoff.

III. Modeling

A. Front Leg Controller Model

In order to examine the stability properties of the unconventional front leg controller, we consider a SLIP-like reduced order model. While the SLIP model is traditionally only used to study a single leg [24], we modify it to examine the front legs' behavior by assuming 1) the effect of the rear legs can be represented as a constant horizontal force 2) the front and rear legs contribute equally to the overall vertical thrust. In order to detect premature touchdown events, a second virtual flight leg was defined and swept at a fixed angular velocity until either touchdown occurred or the desired touchdown angle was reached, as shown in Fig. 4b.

The Equations of Motion (EOM) (Eq. 7 - 9), were determined using Newton's method in Cartesian coordinates. The forces on the COM, the prismatic force F_L and the torsional force F_θ, are defined in polar coordinates by Eq. 8 and the rotated onto the Cartesian frame. *Leg* is a binary flag for stance (1 during stance and 0 for flight). TD occurs when the flight foot is at a height of zero and LO occurs when the force in the leg goes to zero. A step was defined as a stance flight cycle and between strides, Eq. 4 was used to determine the next desired TD angle with Eq. 5 implemented as the safety mechanism.

$$\begin{bmatrix}\ddot{X}\\ \ddot{Y}\end{bmatrix} = \frac{Leg}{m}\begin{bmatrix}\sin(\theta) & -\cos(\theta)\\ 2\cos(\theta) & 2\sin(\theta)\end{bmatrix}\begin{bmatrix}F_L\\ F_\theta\end{bmatrix} + \begin{bmatrix}\frac{Leg\ F_{rear}}{m}\\ -g\end{bmatrix} \tag{7}$$

$$\begin{aligned} F_L &= k(L_{des}-L)+b*(\dot{L}_{des}-\dot{L})\\ F_\theta &= L*[\kappa*(TD_n-\theta)+b_\theta(0-\dot{\theta})]\end{aligned} \tag{8}$$

$$L_{des} = L_0 + \Delta L\sin(2\pi\omega(t-t_{TD})) \tag{9}$$

The simulation study examined the viability of the stability control of Eq. 4 and the safety mechanism of Eq. 5. As such, four values of the front angle gain ($c_1 \in [0.025, 0.05, 0.075, 0.1]$) and four different values for rear force ($F_{rear} \in [2,3,5,10]$)were applied to the model. For each test case, forward simulation was examined (allowing the controller to stabilize to a steady state if possible), with system run for 100 steps and the average velocity and touchdown angle from the last 20 steps were averaged.

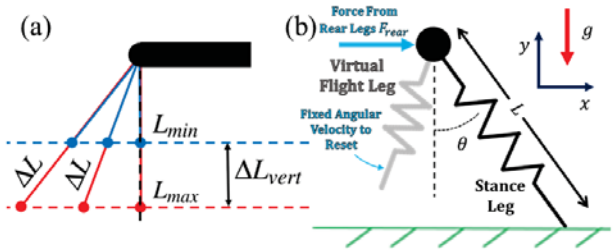

Fig. 4: a) To regulate the pitching moment, the prescribed thrusting motion is modulated to ensure the same travel in the horizontal direction. b). Reduced order simulation of front leg control which models the interaction with the rear leg as a fixed horizontal force. A virtual flight leg is swung at a fixed angular velocity and tracked to determine if touchdown occurs prior to full recirculation.

TABLE I: Model Parameters

Parameter	Symbol	Simulation Values
Mass (kg)	m	5
Nominal Leg Length (m)	L_0	0.2
Spring Stiffness (N/m)	k	2000
Damping (kg/s)	b and b_θ	20 and 3.16
Gravity (m/s^2)	g	9.81
Driving Frequency (Hz)	ω	5.5
Initial TD Angle (°)	TD_{init_f}	20
Vertical Stroke (m)	ΔL_{vert}	0.047
Flight Reset Rate ($^\circ/s$)	$\dot{\theta}_{fl}$	100
Front TD Angle Gain	c_1	0.025,0.05,0.075,0.1
Force from Rear (N)	F_{rear}	2,3,5,10

B. Simulation Results

The primary result from the simulation is that the controller was able to converge to some form of steady state behavior for all values tested. In some cases, the touchdown angle modulation converged to a single touchdown angle, as seen in the case with $c_1 = 0.05$ and $F_{rear} = 3N$ of Fig. 5. In other cases, the system increased velocity until the foot tripped (touchdown occurred prior to full leg recirculation), as seen in the case with $c_1 = 0.05$ and $F_{rear} = 5N$ of Fig. 5. In these cases, the safety mechanism adds a torsional stiffness which imparts a significant braking force causing the system to slow down but maintain forward motion, then eventually increasing speed until the front foot tripped again.

Fig. 5 shows some of the coupled interaction of rear force, controller gain, and tripping. When the system does not trip, the fastest gaits occur with higher controller gain and largest rear force, but once tripping occurs, the fastest gaits occur at lower controller gains and lowest force. Thus for the fastest gaits, we want to increase the controller gain just up to the point were tripping occurs. Although a conservative approximation, this reduced order model suggest that the front leg control scheme is able to stabilize to a steady state and recover from significant perturbations, such as tripping.

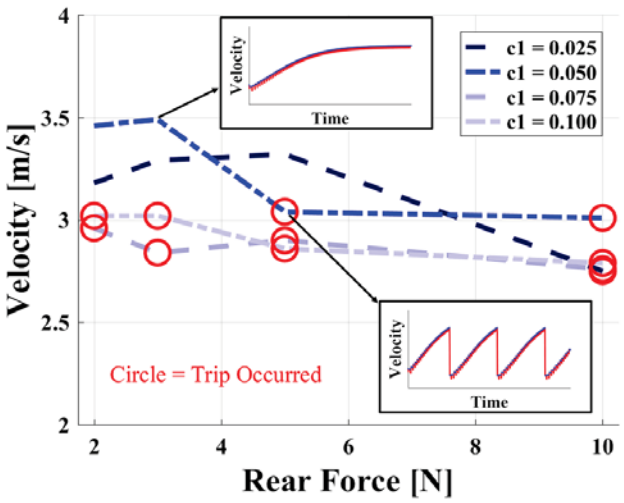

Fig. 5: Simulation Results showing the impact of both components of the front leg controller. The two points highlighted show the COM velocity over the 100 steps, which shows the TD angle can converge to steady state and the reflex torsional stiffness stabilizes the system if it trips.

IV. Experimental Setup

The new trajectory based and LSC controllers were both optimized for speed and then tested on a variety of surfaces to explore the robustness of the controllers. The testing was conducted on two virtually identical robotic platforms, a Minitaur operated by FSU and a Minitaur operated by ARL. The primary difference was the foot design of the FSU version (shown in Fig. 1c).

A. Controller Tuning

1) Tuning Methodology: To equitably compare controllers and reduce variance seen with traditionally used hand tuning techniques, each controller was independently optimized. Nelder-Mead optimization was performed as it has been shown to safely optimize robotic platforms because of its conservative nature [16], [25]. Prior to each optimization, both controllers were hand-tuned to produce viable gaits for the initial simplexes. Additionally, parameter variation from these hand-tuned gaits was utilized to determine the impact of each control parameter on the performance. The optimizations of each controller was performed on a single surface (tile) using FSU's Mintaur which uses the improved elastomer feet. For the optimizations performed in this paper, the cost function was set to $1/velocity$ to produce fast gaits.

2) Trajectory Parameters: The new trajectory controller was specifically designed to be defined by a minimal set of parameters. A complete set of control parameters are shown in Table II along with the optimization bounds and final optimized values. To reduce the wear on the platform, the ground clearance (δ_{clear}) was held constant and the approach length (L_{app}) was defined to maintain a fixed position in the y direction and adjusted based on the approach angle.

The controller gains K_p and K_d are approximations of torsional spring stiffness and damping which traditionally need to be well tuned for optimal performance [26]. Duty factor and actuation frequency together combine to define the velocity along the trajectory at every point. Finally ground clearance, stroke length, and approach angle completely define the shape of the trajectory.

TABLE II: Trajectory Controller Parameters

Parameter	Symbol	Optimization Bounds	Optimized Values
Optimized Parameters			
Actuation Frequency (Hz)	ω	4.5-6.5	6.47
Proportional Control Gain	K_p	0.9-1.8	1.57
Derivative Control Gain	K_d	0.012-0.020	0.013
Duty Factor	$duty$	0.40-0.55	0.48
Stroke Length (cm)	L_{stroke}	14-16	15.6
Approach Angle (°)	β	60-80	62.3
Hand Tuned Parameters			
Ground Clearance (cm)	δ_{clear}	–	10.5
Approach Length (cm)	L_{app}	–	$5.25/\cos(\beta)$

3) LSC Parameters: Based on the unique tasks executed by the front and rear legs, the number of controller parameters for LSC is more than doubled compared with the trajectory controller, as seen in Table III. Prior to optimization, all parameters were individually perturbed to determine the minimum relevant optimization set. The front κ gain, c_2, was determined to be purely a failsafe parameter (which matches the simulation results), and a range of values tested did not significantly impact the steady state performance. The torque ratio threshold, rear angle gain δ, vertical stroke ΔL_{vert}, and initial values for rear torsional stiffness, κ_{init_r}, and TD_{init_f} and TD_{init_r} were determined from the experiments to impact the transient behavior but not the steady state performance.

The parameters that were similar to the trajectory controller were included in the optimization. These include the extension stiffness for the front and rear (comparable to the K_p term in the trajectory controller), the extension and torsional damping (comparable to the K_d term), and the actuator frequency. The parameters which had a significant impact on the steady state performance, the controller gains c_1 and c_3, were also included in the optimization.

B. Performance Evaluation

The controllers were judged on their resulting velocity and their robustness to changing environmental conditions. The controllers' robustness was tested using ARL's Minitaur, which uses stock rubber feet, by varying the surface and the added payload. The specific payload was an additional $1kg$ mass ($\approx 20\%$ body mass) added at COM while running. The range of surfaces were selected to provide distinct variations in environmental conditions. The first surface tested (and the surface the controller optimization was performed on) was tile flooring. Beyond this initial surface, a painted concrete and smooth particle board path were selected to vary the surface friction coefficient, and two thicknesses of foam flooring were selected to vary the surface stiffness and damping. Finally, a compressed gravel pit was used as an extreme surface which would include surface penetration

TABLE III: Leg Specialization Controller Parameters

Parameter	Symbol	Optimization Bounds	Optimized Values
Optimized Parameters			
Actuation Frequency (Hz)	ω	3.5-6.5	5.74
Extension Stiffness Front	k_f	35-350	192.48
Extension Stiffness Rear	k_r	70-350	207.22
Extension Damping	b_{ext}	0.0-0.05	0.003
Torsional Damping	b_{tor}	0.0-0.05	0.003
Front Angle Gain	c_1	0.001-1.0	0.3624
Rear κ gain	c_3	0.001-1.0	0.8341
Hand Tuned Parameters			
Front κ gain	c_2	–	0.3
Torque Ratio Threshold	$Threshold$	–	0.5
Rear Angle Gain	δ	–	0.0075
Vertical Stroke (m)	ΔL_{vert}	–	0.05
Initial κ Rear	κ_{init}	–	0.3
Initial TD Angle Front (°)	TD_{init_f}	–	9
Initial TD Angle Rear (°)	TD_{init_r}	–	-20
Front TD Limit (°)	TD_{limit_f}	–	-20

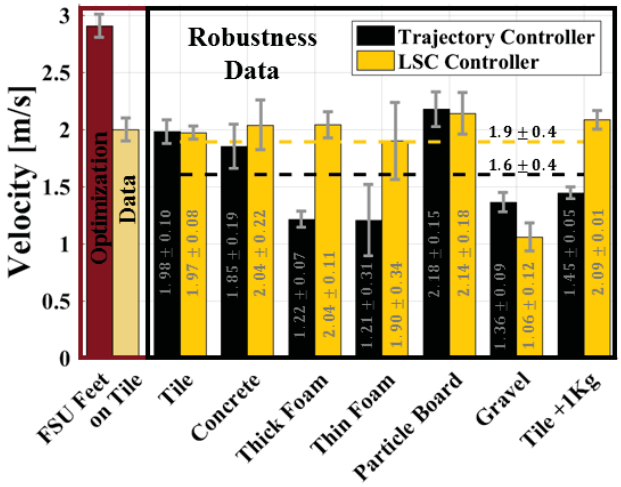

Fig. 6: The experimental results comparing the average velocity achieved with the various environmental changes. The new LSC controller demonstrated significant more robust performance on all surfaces as seen by the average velocity increase of 0.3 m/s

and deformation. Several of these surfaces are shown in Fig. 1b,d-g.

All experiments were recorded with Vicon motion tracking cameras. Each controller/surface combination was tested 5 times with the trials randomized to reduce the potential impact of battery drain and system wear on the performance. The velocity over the final 5 steps of each run were averaged, and these values were then averaged over all the surface trials to determine the velocity on each surface. During experiments, the battery drain was noted, and the battery was replaced when it reached 75% of a full charge. Additionally, the foot wear was examined and new feet were installed every 30 trials regardless of the wear.

V. Experimental Results

A. Optimization Results

The trajectory controller after optimization was able to achieve a top speed of $2.91 \pm 0.1 m/s$. This is an improvement of more than 50% from the previous top speed of $1.9 m/s$ [16], which was achieved on a lighter, but equally powerful version of Minitaur. Examining the optimized control parameters, the stroke length and driving frequency railed high (within bounds of experimental variability). The virtual spring damper converged to unique values away from the optimization boundaries.

The optimization of the Leg Specialization Controller resulted in maximum velocity of $2.00 \pm 0.1 m/s$, which was an improvement from the $1.6 m/s$ achieved via hand tuning. Examining the optimal values, none of the optimized parameters converged near a boundary.

B. Robustness Experimentation

Comparing the controllers robustness, shown in Fig. 6, the velocity of ARL's Minitaur on the original optimized surface resulted in a $0.9 m/s$ reduction in speed for the trajectory based controller, while the LSC controller velocity change was not statistically significant. On the hard surfaces (tile, concrete, and particle board), the difference in velocity between the controllers was marginal. On the foam surfaces modified the effect leg stiffness, the LSC controller was on average $0.76 m/s$ faster than the trajectory controller. The experiments with an added payload resulted in significantly degraded performance for the trajectory controller, which only achieved $1.45 \pm 0.05 m/s$, while the LSC controller actually achieved a marginally higher velocity than its average at $2.09 \pm 0.01 m/s$. The gravel surface caused both systems significant issues. Because of limited track width and no direction control, the robot heading was occasionally influenced by the experimenter. However, this was consistent between controllers. Beyond this, both controllers ran significantly slower than average of the other trials, with the trajectory controller running slightly faster at $1.36 \pm 0.09 m/s$ while the LSC controller only achieved $1.06 \pm 0.12 m/s$.

The dashed lines on Fig. 6 show the average of the velocities over the all the terrains. The LSC controller produced an average velocity of $1.9 \pm 0.4 m/s$ while the trajectory based controller resulted in an average velocity of $1.6 \pm 0.4 m/s$. The standard deviation including every surface results are comparable, but if the gravel terrain is removed, the averages change to 2.0 ± 0.1 and 1.65 ± 0.4.

VI. Discussion

A. Trajectory Improvements

Using the improved re-optimized smoothed trajectory, a new maximum velocity of 2.91 m/s was achieved with Minitaur. In comparing this velocity with past robotic platforms, shown in Table IV, non-dimensional descriptions, such as Froude number ($\frac{V^2}{gL}$) and body lengths per second (BL/s), were determined to be 4.29 and 7.1 respectfully. While smaller platforms (1kg or less), such as Dash [30], UMD's

TABLE IV: 1 kg or larger Quadrupedal Robots Running Performance

Platform	Mass (kg)	Hip Height (m)	Body Length (m)	$V_{max}(m/s)$	Froude Number	$BL/s(s^{-1})$
Fast Quadrupeds						
Scout II [27]	20.8	0.32	0.55	1.30	0.53	2.4
Tekken2 [28]	4.3	0.25	0.30	0.95	0.37	3.2
BigDog [8]	109	1.00	1.10	3.10	0.98	2.8
Rush [29]	4.3	0.20	0.30	0.90	0.41	3.0
HyQ [15]	70	0.68	1.00	2.00	0.60	2.0
ANYmal [9]	30	0.42	0.50	0.80	0.15	1.6
Dynamic Running Robots						
Raibert Quadruped [17]	38	0.56	0.78	2.90	1.53	3.7
Cheetah-Cub [12]	1.1	0.16	0.20	1.42	1.30	6.9
MIT Cheetah II [7]	33	0.48	0.70	6.40	8.70	9.1
Minitaur LSC Controller	5.5	0.20	0.41	2.30	2.70	5.1
Minitaur Trajectory Controller	5.5	0.20	0.41	2.91	4.29	7.1

quadruped [31], and Cheetah-Cub, have been able to achieve high non-dimensional velocities, most larger platforms (5kg or larger), with the exceptions of MIT's Cheetahs, have not achieved Froude numbers greater than 1 (the human walk/run transition).

This improvement over past performance was achieved with a combination of enhancements to the physical system (added splay, improved custom feet) and controller (polynomial splines rather than linear segments), despite an increase in the system mass (without a change in the actuators). Of particular note, the smoothed trajectory controller optimization converged to a lower value for the proportional gain, which suggests the smoothed trajectory enabled better tracking of the desired foot trajectory, which allowed the optimization to use K_p to tune the effective virtual spring stiffness.

B. Controller Comparison

A comparison between the controllers' average velocities demonstrates the LSC controller is significantly more robust to changes in the environment. The average velocities (outside of the gravel experiments), were within $0.1m/s$ of the average. This suggests the functional dynamic decomposition provided sufficient flexibility to adjust leg behavior to different environments. This is especially true with the foam surfaces, which change the surface stiffness, where the trajectory controller's need for a properly tuned spring stiffness was impacted the most.

While the system was significantly more robust to changes in surface, we expected greater performance deviation on surfaces with a higher surface friction (which should enable a larger thrusting force). Therefore, the controller could be significantly improved if foot slipping could be detected.

C. Platform Robustness

During experimentation, the amount of foot wear and recovery from random perturbations were recorded visually. The trajectory controller required a new set of rubber feet after every 30 trials, while the same wear was never achieved with the LSC controller. In addition to increasing the rate of wear, the trajectory controller's performance decreased by as much as 10% as the foot approached the point of replacement while the LSC's performance remained within experimental noise. This was occasionally coupled with battery drain, which would reduce the trajectory controller's performance by as much as 20%, while the LSC controller's performance was impacted by less than 10%.

The trajectory controller also operates in a more dangerous region for the motors. The optimization of the trajectory converged to the limits of driving frequency and stroke length, which were both defined by motor limits. During the optimization of the trajectory controller, two motors were burned out, while the LSC controller's entire optimization was run without damaging any motor. It is interesting to note that the LSC controller's optimization did not converge to the limit of driving frequency as the fastest speeds are generally achieved by maximizing stride length and stride frequency. This suggests the lower frequency gaits enabled greater thrust to be provided by the rear legs which increased the stride length.

D. Controller Limits

While the controllers were generally able to traverse the various terrains successfully, neither controller handled the gravel terrain particularly well. This is likely due to both controllers being designed with the assumption of a fixed terrain (no surface penetration). Both controllers had the foot slip within the surface and thus lose energy, which the torque ratio would not capture with an encapsulated foot. The trajectory controller did perform better, which is likely tied to a higher foot clearance during stance compared with the LSC controller.

VII. Conclusion

In this paper, a new quadrupedal controller was developed using the concept of functional leg specialization. The controller adjusts the leg touchdown angle and torsional stiffness of the front and rear legs independently to provide as much forward speed as possible, while safety mechanisms (demonstrated via simulation) extend the stability limits.

This new controller (LSC controller) was then implemented on Minitaur and directly compared with an improved trajectory controller. The improved trajectory controller produced the highest velocity seen with Minitaur, and one of the highest velocities in terms of body lengths per second of any platform over 5kg. However, the new LSC control was shown to be significantly more robust to changes in terrain and changing payload.

While the particular formulations of the LSC controller outlined in this paper is effective, alternative formulations may be possible and may be more effective on rough terrain. Improvements in slip detection, pitch regulation, and mechanical specialization of the legs (e.g. larger more powerful rear legs) may improve the robot's performance. In addition, a more detailed analysis of the coupled front rear dynamics may help refine to how fore-aft leg specialization can be used to produce even faster, more stable and more efficient gaits.

ACKNOWLEDGMENTS

We would like to thank Matthew Davis, David Balbuena, and Jorge Campa for their work in assisting with performing the experiments conducted in this work and Chip Young for his work developing and manufacturing the elastomer feet. This work was supported by the collaborative participation in the Robotics Consortium sponsored by the U.S. Army Research Laboratory under the Collaborative Technology Alliance Program, Cooperative Agreement DAAD 19-01-2-0012, and by NSF Grant CMMI-1351524. The U.S. Government is authorized to reproduce and distribute reprints for Government purposes not withstanding any copyright notation thereon.

REFERENCES

[1] R. M. Alexander, *Principles of animal locomotion*. Princeton University Press, 2003.

[2] M. Raibert, *Legged Robots that Balance*, ser. Artificial Intelligence. MIT Press, 1986. [Online]. Available: https://books.google.com/books?id=EXRiBnQ37RwC

[3] G. A. Cavagna, N. C. Heglund, and C. R. Taylor, "Mechanical work in terrestrial locomotion: two basic mechanisms for minimizing energy expenditure," *American Journal of Physiology-Regulatory, Integrative and Comparative Physiology*, vol. 233, no. 5, pp. R243–R261, 1977.

[4] R. Blickhan, "The spring-mass model for running and hopping," *Journal of Biomechanics*, vol. 22, no. 11-12, pp. 1217–1227, Jan. 1989.

[5] B. Andrews, B. Miller, J. Schmitt, and J. E. Clark, "Running over unknown rough terrain with a one-legged planar robot," *Bioinspiration & biomimetics*, vol. 6, no. 2, p. 026009, 2011.

[6] A. Seyfarth, H. Geyer, and H. Herr, "Swing-leg retraction: a simple control model for stable running," *Journal of Experimental Biology*, vol. 206, no. 15, pp. 2547–2555, 2003.

[7] H.-W. Park, P. M. Wensing, and S. Kim, "High-speed bounding with the mit cheetah 2: Control design and experiments," *The International Journal of Robotics Research*, vol. 36, no. 2, pp. 167–192, 2017.

[8] M. Raibert, K. Blankespoor, G. Nelson, R. Playter *et al.*, "Bigdog, the rough-terrain quadruped robot," in *Proceedings of the 17th World Congress*, vol. 17, no. 1, 2008, pp. 10 822–10 825.

[9] M. Hutter, C. Gehring, D. Jud, A. Lauber, C. D. Bellicoso, V. Tsounis, J. Hwangbo, K. Bodie, P. Fankhauser, M. Bloesch *et al.*, "Anymal-a highly mobile and dynamic quadrupedal robot," in *Intelligent Robots and Systems (IROS), 2016 IEEE/RSJ International Conference on*. IEEE, 2016, pp. 38–44.

[10] G. Kenneally, A. De, and D. E. Koditschek, "Design principles for a family of direct-drive legged robots," *IEEE Robotics and Automation Letters*, vol. 1, no. 2, pp. 900–907, July 2016.

[11] H. Cruse, T. Kindermann, M. Schumm, J. Dean, and J. Schmitz, "Walknet?a biologically inspired network to control six-legged walking," *Neural networks*, vol. 11, no. 7, pp. 1435–1447, 1998.

[12] A. Spröwitz, A. Tuleu, M. Vespignani, M. Ajallooeian, E. Badri, and A. J. Ijspeert, "Towards dynamic trot gait locomotion: Design, control, and experiments with cheetah-cub, a compliant quadruped robot," *The International Journal of Robotics Research*, vol. 32, no. 8, pp. 932–950, 2013.

[13] D. J. Hyun, S. Seok, J. Lee, and S. Kim, "High speed trot-running: Implementation of a hierarchical controller using proprioceptive impedance control on the mit cheetah," *The International Journal of Robotics Research*, vol. 33, no. 11, pp. 1417–1445, 2014.

[14] M. Hutter, C. D. Remy, M. A. Hoepflinger, and R. Siegwart, "Efficient and versatile locomotion with highly compliant legs," *IEEE/ASME Transactions on Mechatronics*, vol. 18, no. 2, pp. 449–458, 2013.

[15] C. Semini, N. G. Tsagarakis, E. Guglielmino, M. Focchi, F. Cannella, and D. G. Caldwell, "Design of hyq–a hydraulically and electrically actuated quadruped robot," *Proceedings of the Institution of Mechanical Engineers, Part I: Journal of Systems and Control Engineering*, vol. 225, no. 6, pp. 831–849, 2011.

[16] M. Austin, J. M. Brown, K. Geidel, W. Wang, and J. E. Clark, "Gait design and optimization for efficient running of a direct-drive quadrupedal robot," in *SPIE Defense+ Security*, 2017.

[17] M. H. Raibert, "Trotting, pacing and bounding by a quadruped robot," *Journal of biomechanics*, vol. 23, pp. 7983–8198, 1990.

[18] R. J. Full, R. Blickhan, and L. Ting, "Leg design in hexapedal runners," *Journal of Experimental Biology*, vol. 158, no. 1, pp. 369–390, 1991.

[19] J. Chen, A. Peattie, K. Autumn, and R. Full, "Differential leg function in a sprawled-posture quadrupedal trotter," *Journal of Experimental Biology*, vol. 209, no. 2, pp. 249–259, 2006.

[20] J. G. Cham, S. A. Bailey, J. E. Clark, R. J. Full, and M. R. Cutkosky, "Fast and robust: Hexapedal robots via shape deposition manufacturing," *The International Journal of Robotics Research*, vol. 21, no. 10-11, pp. 869–882, 2002.

[21] J. E. Clark and M. R. Cutkosky, "The effect of leg specialization in a biomimetic hexapedal running robot," *Journal of dynamic systems, measurement, and control*, vol. 128, no. 1, pp. 26–35, 2006.

[22] S. Kim, J. E. Clark, and M. R. Cutkosky, "isprawl: Design and tuning for high-speed autonomous open-loop running," *The International Journal of Robotics Research*, vol. 25, no. 9, pp. 903–912, 2006.

[23] D. J. Blackman, J. V. Nicholson, C. Ordonez, B. D. Miller, and J. E. Clark, "Gait development on minitaur, a direct drive quadrupedal robot," in *SPIE Defense+ Security*. International Society for Optics and Photonics, 2016, pp. 98 370I–98 370I.

[24] R. Blickhan, "The spring-mass model for running and hopping," *Journal of biomechanics*, vol. 22, no. 11-12, pp. 1217–1227, 1989.

[25] J. D. Weingarten, G. A. Lopes, M. Buehler, R. E. Groff, and D. E. Koditschek, "Automated gait adaptation for legged robots," in *Robotics and Automation, 2004. Proceedings. ICRA'04. 2004 IEEE International Conference on*, vol. 3. IEEE, 2004, pp. 2153–2158.

[26] K. C. Galloway, J. E. Clark, M. Yim, and D. E. Koditschek, "Experimental investigations into the role of passive variable compliant legs for dynamic robotic locomotion," in *Robotics and Automation (ICRA), 2011 IEEE International Conference on*. IEEE, 2011, pp. 1243–1249.

[27] I. Poulakakis, J. A. Smith, and M. Buehler, "Modeling and experiments of untethered quadrupedal running with a bounding gait: The scout ii robot," *The International Journal of Robotics Research*, vol. 24, no. 4, pp. 239–256, 2005.

[28] H. Kimura, Y. Fukuoka, and A. H. Cohen, "Adaptive dynamic walking of a quadruped robot on natural ground based on biological concepts," *The International Journal of Robotics Research*, vol. 26, no. 5, pp. 475–490, 2007.

[29] Z. Zhang and H. Kimura, "Rush: a simple and autonomous quadruped running robot," *Proceedings of the Institution of Mechanical Engineers, Part I: Journal of Systems and Control Engineering*, vol. 223, no. 3, pp. 323–336, 2009.

[30] P. Birkmeyer, K. Peterson, and R. S. Fearing, "Dash: A dynamic 16g hexapedal robot," in *Intelligent Robots and Systems, 2009. IROS 2009. IEEE/RSJ International Conference on*. IEEE, 2009, pp. 2683–2689.

[31] C. Y. Brown, D. E. Vogtmann, and S. Bergbreiter, "Efficiency and effectiveness analysis of a new direct drive miniature quadruped robot," in *Robotics and Automation (ICRA), 2013 IEEE International Conference on*. IEEE, 2013, pp. 5631–5637.